(Received 10 October 2025, Accepted 3 December 2025, Scheduled 17 December 2025)

High Gain and Bandwidth Enhanced Microstrip Patch Antenna with Defective Ground Structure Loaded with Metamaterial Unit Cells for Intelligent Transportation Systems

Sunil K. Dubey[1], Ashok K. Shankhwar[1], Nand Kishore[1], and Alkesh Agrawal[2,*]

[1] *Harcourt Butler Technical University, Nawabganj, Kanpur 208002, U.P., India*
[2] *Shri Ramswaroop Memorial University, Barabanki 225003, U.P., India*

ABSTRACT: In the manuscript, a novel design of microstrip patch antenna with moderate degree of complexity is proposed in terms of metamaterial based unit cells as a radiating patch on the top as well as metamaterial based periodic structure as defected ground structure at the bottom (MRPMGS) for Intelligent Transportation System (ITS) applications. The novel design of patch antenna exhibited multi-bands with broad-band transmission patterns, improved high gain, high radiation efficiency, and compact structure. The MRPMGS has a three layered structure with overall dimensions of 32 mm × 28 mm × 1.6 mm. The top layer with radiating patch has unit cells with dimensions of 3.6 mm × 3.6 mm, and at the bottom the defective ground structure (DGS) has unit cells with dimensions of 4 mm × 4 mm. The middle layer is of an FR4 substrate with 1.6 mm thickness. The MRPMGS has experimental (simulated) transmission frequencies at 11.54 GHz (11.24 GHz), 12.91 GHz (12.98 GHz), and 13.20 GHz (13.48 GHz) with reflection coefficients of −20.91 dB (−25.16 dB), −26.19 dB (−29.36 dB), and −18.94 dB (−26.02 dB), respectively. The VSWR varies between 1 and 3. The radiation efficiency reaches 80%, and high gain varying between 2.35 and 5.5 is achieved at the desired frequencies.

1. INTRODUCTION

As wireless communication has advanced, research into microstrip antennas has become more and more popular due to their thin, planar shape and simplicity in surface attachment on missiles and airplanes [1, 2], simplicity of integration, especially in mobile radio communication devices, with other components on the same printed board [3–5]. A triple layered patch antenna, which has a square [6], circular [7], rectangular [8], elliptical [9], or any continuous shaped patch [10] on top with a matching feedline and a bottom ground plane layer separated by a substrate layer, is the most often used type of microstrip antenna. Microstrip patch antennas are widely used in WiMax [11, 12], GPS [9, 10], mobile devices [13], WLAN [9–12], and Intelligent Transportation Systems [14, 15]. Patch antennas were found to have low gain, limited power handling capacity, high feed network losses, and narrow bandwidth [8–11].

Numerous strategies have been put out to address these issues, such as thickening the substrate, incorporating slots on the patch, and developing defective ground structures (DGSs) based on new concept of metamaterial based unit cells [16, 17]. Repetition of a structure like fractals [18], metamaterial based unit cells [19], and the implementation of patches or slots [20] in antennas tend to decrease their physical dimensions and produce resonant qualities that exhibit multi-band and wide-band responses [21]. Using repetitive patterns of metamaterial unit cells for creating slits inside the overall radiating patch and ground structure (DGS) results in the reduction in mutual interference between neighboring antennas, suppressing side lobes and providing high gain and increased bandwidth [22, 23]. The presented research work is focused on a novel design of microstrip patch antenna with metamaterial based unit cells as radiating patch on the top as well as metamaterial based unit cells in the ground plane acting as DGS with applications in ITS.

For the past few years a significant amount of research has been done to enhance patch antennas' performance and design, miniaturize the antenna design, improve radiation pattern of transmitting antenna, and enhance frequency and bandwidth response by introducing a new concept of metamaterial unit cells based radiating patches [24] and metamaterial unit cells based DGS [25].

A new class of materials that are not found naturally is termed as "metamaterials" (MMs). The electromagnetic (EM) properties of these artificially designed materials are distinct from those of naturally occurring materials, such as effective permittivity (ε_{eff}) and effective permeability (μ_{eff}) values below zero [26], where unique electromagnetic properties are exhibited by the structural unit cell orientation, periodic arrangement, and the shape instead of directly inheriting these properties from the composition of the material or lattice structure. Pendry et al. [27] reported two prominent artificial structures, arrangement of split ring resonators (SRRs) exhibiting effective permeability (μ_{eff}) < 0 and periodic structured micro wires exhibiting negative value of effective permittivity (ε_{eff}) below plasma frequency (ω_p). A plasma is a density wave of electron gas. Smith et al. [28] showed a composite medium made up of micro-structured wires and a periodic arrangement of SRRs,

* Corresponding author: Alkesh Agrawal (alkesh.agrawal26@gmail.com).

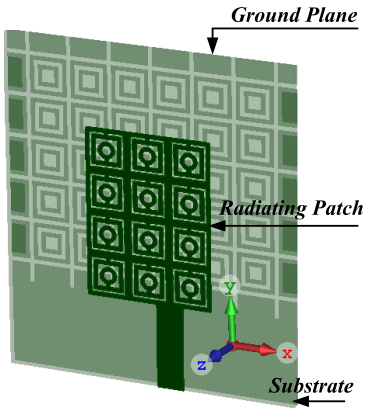

FIGURE 1. 3D view of the MRPMGS antenna.

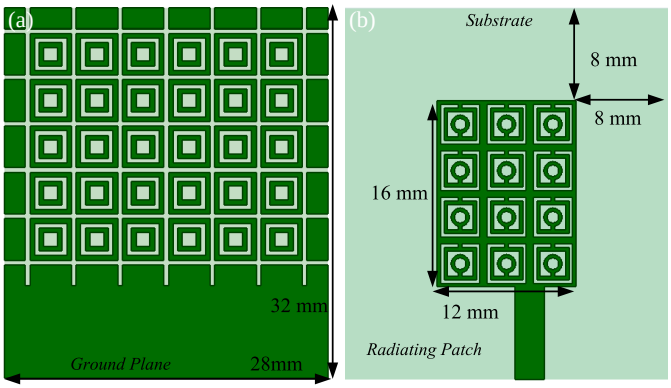

FIGURE 2. MRPMGS antenna view. (a) From bottom. (b) From top.

which exhibited negative value of effective permittivity (ε_{eff}) and effective permeability (μ_{eff}).

Alqadami et al. [16] proposed a patch antenna with an SRR based ground structure that exhibits multi-band frequency response, improved gain, and efficiency as compared to conventional ground plane. Mishra and Chaudhary [17] proposed a patch antenna array with metamaterial based patches. It exhibited improved bandwidth of the frequency band as compared to simple patches. Song et al. [19] proposed an antenna that consists of a 2-element array, with each unit being a patch antenna loaded with six uniformly sized complementary split ring resonators (CSRRs). It exhibited improved reflection coefficient and enhanced bandwidth response. Mood and Pandeeswari [21] proposed a compact design antenna with a continuous folded metamaterial (CFL-MTM) based radiating patch, in contrast to a traditional patch antenna, with a miniature structure and broad-band response. Upadhyay et al. [22] proposed a dual feed patch antenna with a CSRR-loaded centre-fed patch. The antenna exhibited multi-band response, enhanced bandwidth and gain. Upadhyay et al. [25] proposed a microstrip patch antenna with a ground structure consisting of a metamaterial based unit cell. It exhibited broad-band frequency response with very low values of reflection coefficients. Selvi et al. [29] proposed an SRR inspired patch antenna, where the SRR loaded antenna attained enhanced bandwidth of dual bands. Hassan et al. [30] proposed a Ka dual-band antenna with high gain and efficiency with omnidirectional radiation patterns loaded with a metamaterial based radiating patch top layer.

2. MRPMGS ANTENNA DESIGN

The proposed MRPMGS antenna design is a typical three layered novel structure where the top layer consists of 2D periodic array of metamaterial unit cells as radiating patch; the ground plane is a defected ground structure that also consists of 2D periodic array metamaterial unit cells; and the middle layer is an FR4 substrate as shown in Fig. 1. The DGS and overall dimensions of the MRPMGS antenna are $l_1 \times b_1$ (32 mm $\times$ 28 mm), and the top layer radiating surface has the dimensions of $l_2 \times b_2$ (16 mm$\times$12 mm) as shown in Figs. 2(a) and 2(b). The structural unit of the top layer of the MRPMGS antenna is a metamaterial unit cell with three ring resonators where outer and middle resonators are square in shape, and inner most resonator is ring structured as shown in Fig. 3(a). The dimension of outer most square resonator is x_3 by y_3 (4 mm $\times$ 4 mm), and middle square resonator is x_4 by y_4 (2.8 mm $\times$ 2.8 mm). The inner most ring resonator has outer radius of r_1 (0.8 mm). In order to generate the periodic array of unit cells on the top rectangular patch of 12 mm by 16 mm, three different shaped patches are etched out. The first continuous ring resonator (CRR) patch is generated by subtracting square patch-1 (3.2 mm by 3.2 mm) from square patch-2 (4 mm by 4 mm). The second CRR is generated by subtracting square patch-3 (2 mm by 2 mm) from square patch-4 (2.8 mm by 2.8 mm). The third CRR is generated by subtracting circular patch-1 of diameter 0.5 from circular patch-2 of diameter 0.8 mm. Finally the so obtained differently shaped patches are subtracted from the rectangular patch of 12 mm by 16 mm. The structural unit of ground plane is also metamaterial unit cells with concentric square shaped ring resonators shown in Fig. 3(b). The dimension of the outer square ring resonator is x_1 by y_1 (4 mm $\times$ 4 mm). The dimension of the inner square ring resonator is x_2 by y_2 (2.8 mm $\times$ 2.8 mm). The dimensional parameters are depicted in Table 1.

TABLE 1. Dimensional parameters of the MRPMGS antenna.

Parameter	Dimension (mm)	Parameter	Dimension (mm)
l_1	32	x_2	2.8
b_1	28	y_2	2.8
l_2	16	g_1	0.4
b_2	12	g_2	0.4
l_3	8	w_1	0.4
b_3	2.5	x_3	4
l_4	8	y_3	4
b_4	7.5	x_4	2.8
b_5	8	y_4	2.8
x_1	3.6	g_3	0.3
y_1	3.6	w_2	0.3

MRPMGS antenna design is optimized in steps shown in Figs. 4(a)–4(d), using Equations (1)–(3) [31]. For an antenna with a rectangular patch, W is the width of the patch which should be less than λ_o (wavelength of free space), and L is the

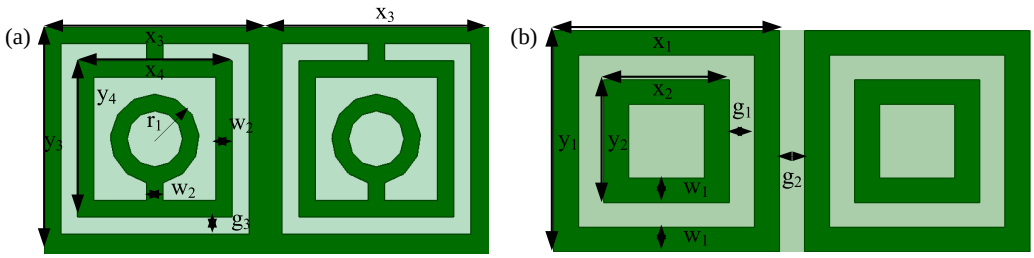

FIGURE 3. (a) Structural unit on top. (b) Structural unit at the bottom of MRPMGS antenna.

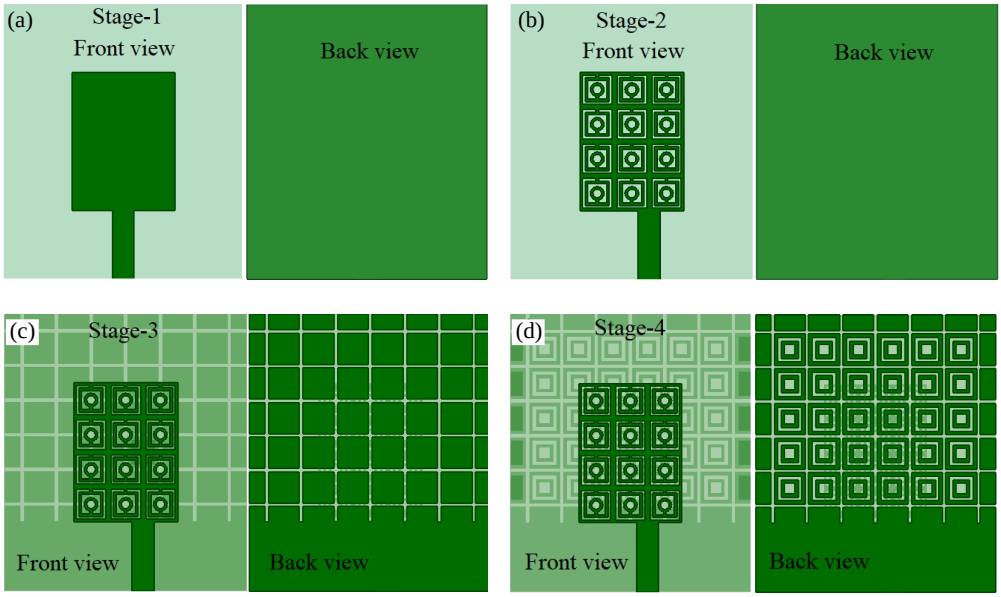

FIGURE 4. (a) Conventional patch antenna in Stage-1. (b) Metamaterial based radiating patches in Stage-2. (c) Defective ground structure in Stage-3. (d) Metamaterial based ground structure in Stage-4 of proposed MRPMGS antenna.

patch length ($\lambda_o/3 < L < \lambda_o/2$), which regulates the antenna frequency, but these parameters cannot be beyond the limits; otherwise the antenna behaves as a microstrip line and not as a radiator [13]. The patch antenna's input resistance is controlled by its width.

Equation (1) [31] governs the width of the patch antenna as:

$$W = \frac{1}{2f_o\sqrt{\mu_o\varepsilon_0}}\sqrt{\frac{2}{\varepsilon_r+1}} \tag{1}$$

where f_o is the resonating frequency; ε_r is the permittivity of the substrate; μ_o and ε_o are the permeability and permittivity of the free space.

Equation (2) [31] depicts the effective dielectric constant:

$$\varepsilon_r = \frac{\varepsilon_r+1}{2} + \left(\frac{\varepsilon_r-1}{2}\right)\left[1+12\left(\frac{h}{W}\right)\right]^{\frac{-1}{2}} \tag{2}$$

where h is the substrate height.

Equation (3) [31] is utilized to compute the patch's extended length as a result of the fringing field.

$$\frac{\Delta L}{h} = 0.412\left[\frac{\left(\varepsilon_r^{eff}+0.3\right)\left(\frac{W}{h}+0.264\right)}{\left(\varepsilon_r^{eff}-0.258\right)\left(\frac{W}{h}+0.8\right)}\right] \tag{3}$$

where ΔL is the "Fringing length extension" added to each edge of the patch to get an "effective length" L_e [31].

In Stage-1, a conventional rectangular patch antenna is designed using Equations (1)–(3). Stage 2 is evolved by converting the traditional radiating patch into a periodic array of metamaterial unit cells. In Stage-3, the ground plane is converted into a defected ground structure by generating horizontal and vertical slits. Finally in Stage-4, the DGS is also transformed into a $2d$ periodic array of metamaterial unit cells as shown in Figs. 4(a)–4(d).

Figures 5(a) and 5(b) show the equivalent circuit model of the metamaterial based unit cell patch on the top layer of MRPMGS antenna and bottom layer ground plane, respectively. In order to better understand the response of the proposed MRPMGS antenna structure, the equivalent circuit model is developed as shown in Figs. 5(a) and 5(b). The top layer radiating patch consists of unit cells structure, each cell consists of three resonator structures, and each resonator structure is depicted with R, L, and C circuits separated by the coupling capacitance for the gap in between resonator patches. The two resonators are mutually coupled with each other and in turn coupled with the third resonator patch as depicted in Fig. 5(a). Similarly, the ground plane has two resonators that are mutually coupled and

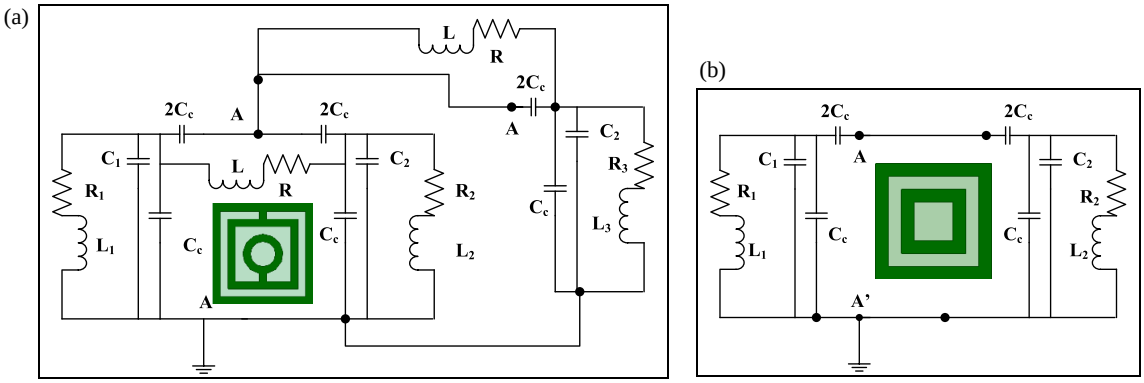

FIGURE 5. (a) Equivalent circuit model of metamaterial based unit cell patch on top. (b) Equivalent circuit model of metamaterial based unit cell patch in ground plane.

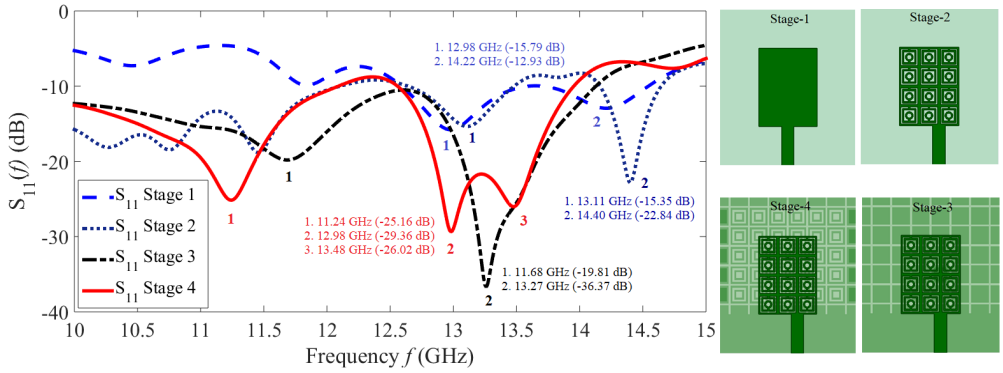

FIGURE 6. Comparison of the proposed antenna's S_{11} response for four stages.

also depicted with R, L, and C elements with coupling capacitors to model the gap in between as shown in Fig. 5(b).

3. MRPMGS ANTENNA SIMULATION

Computational electromagnetics software "CST Microwave Studio" is used to simulate the optimal MRPMGS antenna design, splitting the structure into 588,570 hexahedral mesh cells. In all three directions (x, y, and z), open boundary conditions are fixed. The antenna design is modified and optimized stage by stage, and the response is simulated for each stage till the desired response is obtained after Stage-4. Fig. 6 depicts the response of all the four stages. The optimized MRPMGS antenna resonates at 11.24 GHz, 12.98 GHz, and 13.48 GHz. The 2nd and 3rd resonant frequencies merged to get a broad-band response of 1.50 GHz as shown in Fig. 6. This response is obtained due to the novel concept of metamaterial based 2D periodic array of radiating patches on the top as well as metamaterial based 2D periodic array of ground structure. Metamaterial unit cells of the 2D periodic array on the top interact with each other creating a combined resonating effect whereas the ground plane with metamaterial based 2D periodic array minimizes the side lobes and improves the transmission response of the antenna.

Figures 7 and 8 illustrate how the power is supplied to port 1 from the feed line that creates surface currents on the patch at the top layer and ground plane at the bottom, respectively. Electric and magnetic fields are further induced by the induced surface current distributions [25], and the confined surface currents inside the antenna construction are transformed into electromagnetic waves in accordance with the maximum power transfer theorem. As a result, the highest radiation of the suggested MRPMGS occurs at 11.24 GHz, 12.98 GHz, and 13.48 GHz. Wide-band response is the result of the transverse magnetic mode radiation produced by the metamaterial-based unit cells patch on the top in combination with the transverse magnetic mode radiation produced by the metamaterial-based unit cells on ground plane [25] (depicted in Fig. 6).

Another important parameter in the good design of an antenna is Voltage Standing Wave Ratio (VSWR). The degree of mismatch between an antenna and the feed line that connects to it is indicated by VSWR, also termed as standing wave ratio (SWR). The VSWR value range is 1 to ∞. For a good antenna design application, a VSWR value of less than two is assumed to be most appropriate. Fig. 9 depicts the simulated VSWR for the proposed MRPMGS antenna. It clearly indicates that at the desired range of frequencies the VSWR is between 1 and 3, which points towards a good design of the proposed antenna with optimized dimensions. Another parameter known as antenna gain quantifies how much of an antenna's radiation pattern, or angular distribution of radiated power, is concentrated in a single direction. With a focused, restricted beamwidth, a high-gain antenna (HGA) is a directional antenna that allows for more accurate radio signal targeting. Fig. 10 depicts the

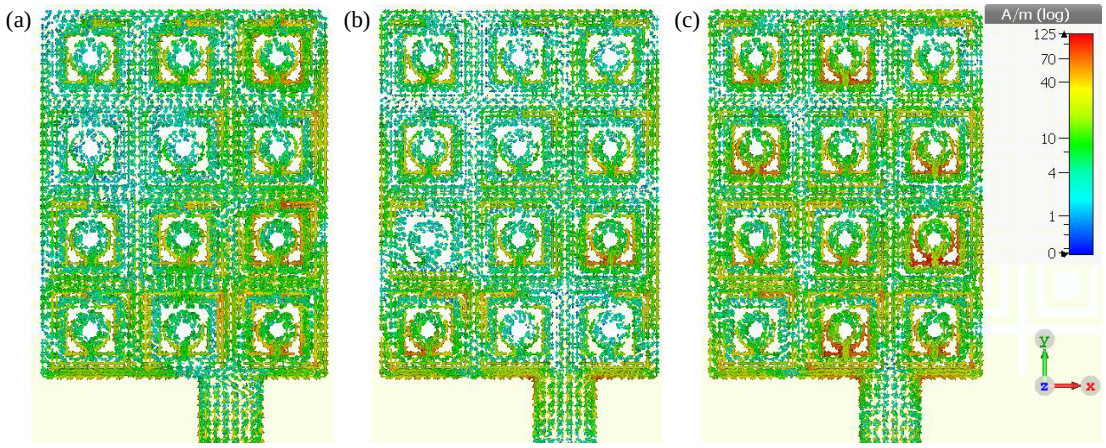

FIGURE 7. Current distributions on top surface (a) at 11.24 GHz, (b) at 12.98 GHz, (c) at 13.48 GHz.

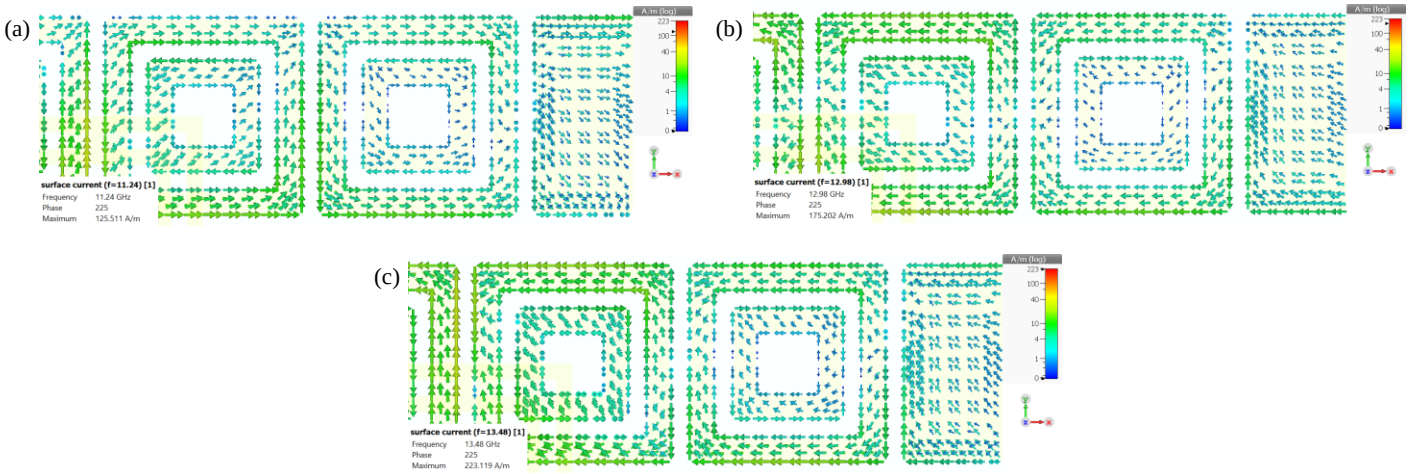

FIGURE 8. Current distributions at the ground plane surface (a) at 11.24 GHz, (b) at 12.98 GHz, (c) at 13.48 GHz.

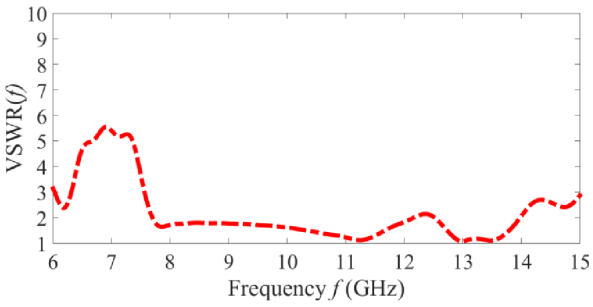

FIGURE 9. VSWR for the proposed MRPMGS antenna.

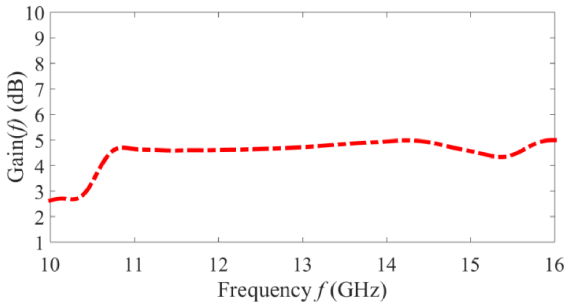

FIGURE 10. Gain $G(f)$ for the proposed MRPMGS antenna.

gain of the antenna over the range of frequencies from 10 GHz to 16 GHz. It shows unequivocally that the antenna gain ranges from 3 to 5 for frequencies between 10 GHz and 16 GHz.

4. METAMATERIAL BEHAVIOUR OF RADIATING PATCHES AND DEFECTIVE GROUND STRUCTURE

The radiating patch and the ground plane loaded with metamaterial-based unit cells are what make the MRPMGS antenna unusual in terms of structure. The metamaterial behavior is studied in terms of the normalized effective impedance, effective permeability, and effective permittivity calculated using Equations (4)–(6) [32]. The normalized effective impedance for the metamaterial unit cell based radiating patch is shown in Fig. 11(a), and that of defective ground structure in Fig. 12(a) clearly depicts that under perfectly matched conditions, $\mathrm{Re}(Z(f)) \approx 1$ and $\mathrm{Im}(Z(f)) \approx 0$. The effective permeability and permittivity for metamaterial unit cell based radiating patch are shown in Figs. 11(b) and 11(c), respectively,

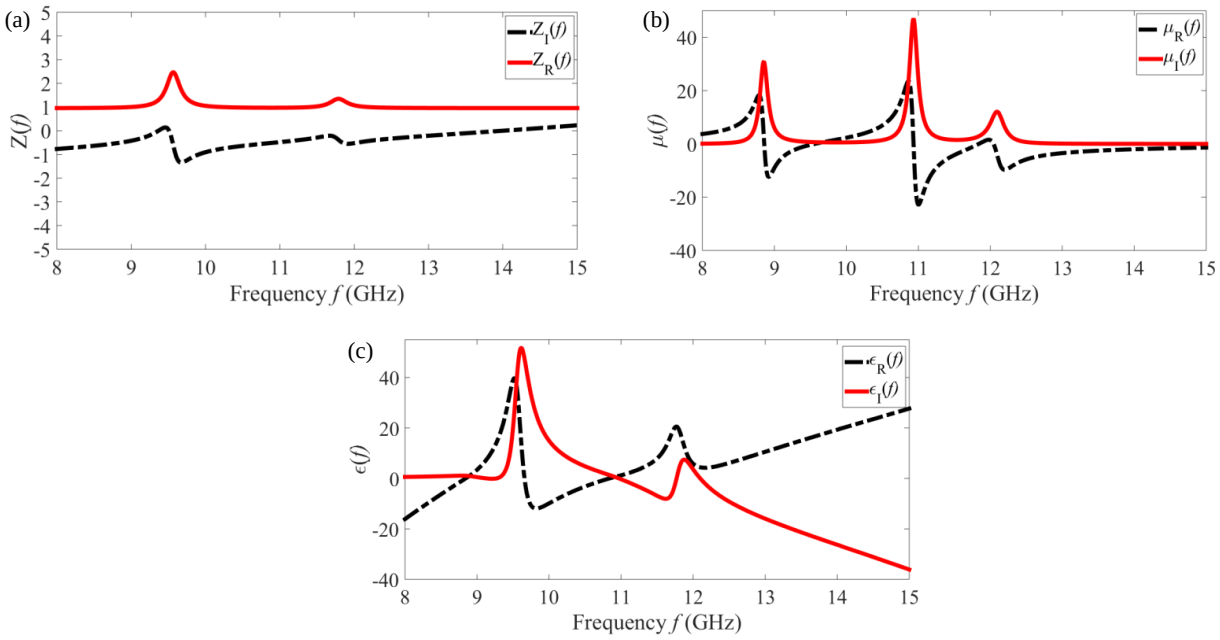

FIGURE 11. (a) Normalized effective impedance. (b) Effective permeability. (c) Effective permittivity of metamaterial based radiating patch.

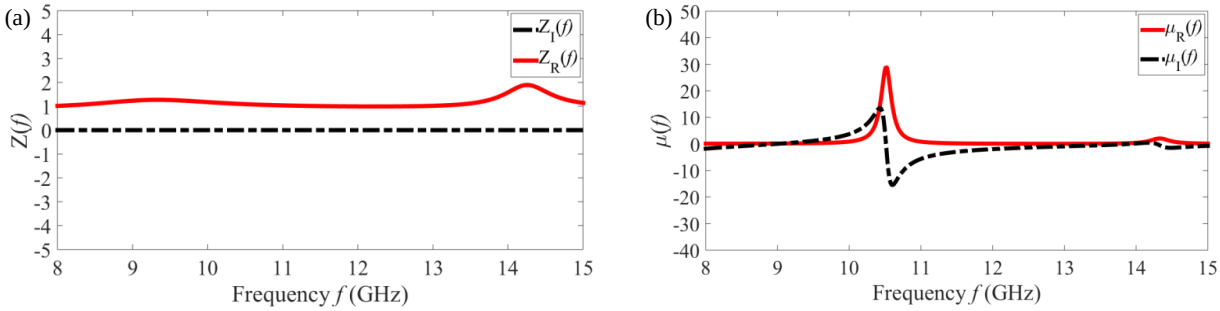

FIGURE 12. (a) Normalized effective impedance. (b) Effective permeability of metamaterial based defective ground structure.

whereas the effective permeability for metamaterial unit cell based defective ground structure is shown in Fig. 12(b) and depicts Lorentzian transitions. At Lorentzian transitions, where the effective real permeability and permittivity cross zero values, the imaginary values hold high values.

$$Z_{eff} = \sqrt{\frac{(1+S_{11})^2 - S_{21}^2}{(1-S_{11})^2 - S_{21}^2}} \tag{4}$$

$$\mu_{eff} = \frac{2}{jk_o d}\left(\frac{1+S_{11}-S_{21}}{1-S_{11}+S_{21}}\right) \tag{5}$$

$$\epsilon_{eff} = \frac{2}{jk_o d}\left(\frac{1-S_{11}-S_{21}}{1+S_{11}+S_{21}}\right) \tag{6}$$

Z_{eff} is the effective normalized matched impedance, μ_{eff} the effective permeability, ε_{eff} the effective permittivity, and S_{11} and S_{21} are the reflection and transmission coefficients, respectively, in Equations (4)–(6).

5. EXPERIMENT AND RESULTS

The MRPMGS antenna structure is fabricated on a double sided copper laminated FR-4 substrate (relative permittivity 4.4, loss tangent 0.02 and thickness 1.6 mm) by photolithographic method followed by wet etching process [25] with radiating patch dimensions 16 mm × 12 mm shown in Fig. 13(a) and ground plane dimensions 32 mm × 28 mm as shown in Fig. 13(b). The novelty in the fabricated design is the metamaterial unit cells loaded radiating patch as well as the metamaterial unit cells loaded defected ground structure. Horn antenna and a Vector Network Analyzer (VNA) are used to experimentally evaluate the fabricated MRPMGS antenna in an anechoic environment. As shown in Fig. 14(a), to observe the input reflection coefficient, port 1 of the VNA is connected to the SMA connector of the MRPMGS antenna. Table 2 shows the comparison of simulated and experimentally measured S_{11} of MRPMGS antenna. To calculate the far field, the fabricated antenna is positioned within an anechoic chamber. The placement of the MRPMGS antenna in front of the horn antenna on a revolving disc machine is depicted in Fig. 14(b). The rotating disc machine at the microwave lab is

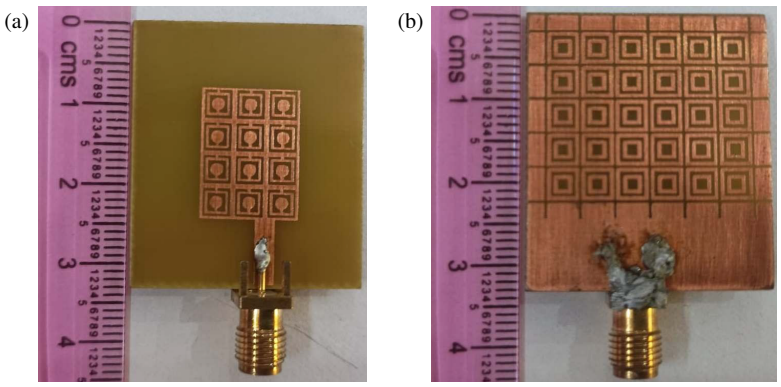

FIGURE 13. (a) Top view of fabricated MRPMGS antenna. (b) Bottom view of fabricated MRPMGS antenna.

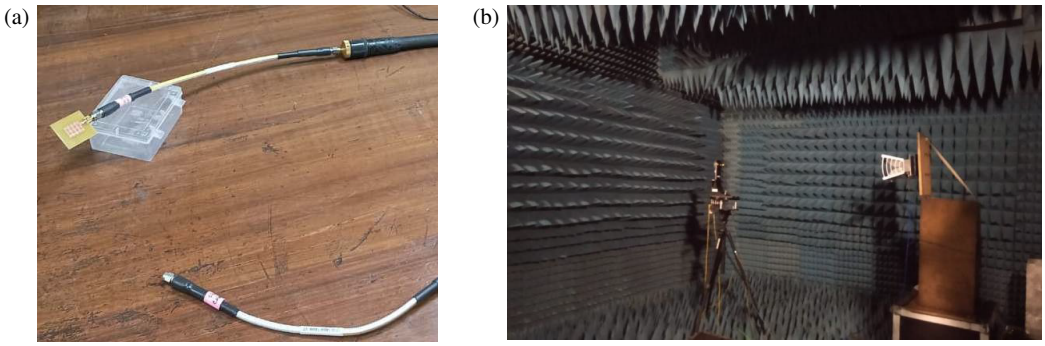

FIGURE 14. (a) Top view of fabricated MRPMGS antenna. (b) Bottom view of fabricated MRPMGS antenna.

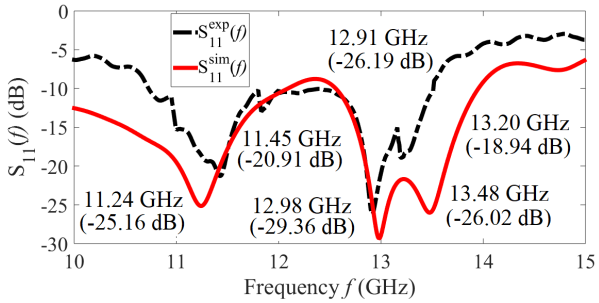

FIGURE 15. Simulated and experimentally measured S_{11} of MRPMGS antenna.

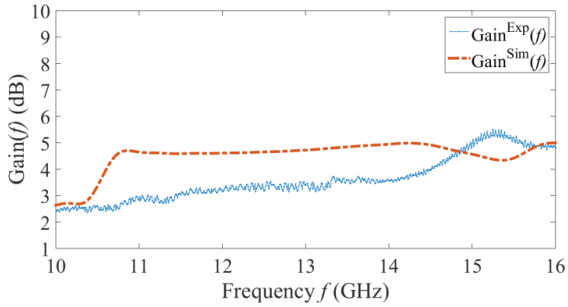

FIGURE 16. Experimentally measured and simulated gains of the MRPMGS antenna.

TABLE 2. Comparison of simulated and experimentally measured S_{11} of MRPMGS antenna.

Simulated Results		**Experimental Results**	
Resonance Frequency (GHz)	S_{11} **(dB)**	**Resonance Frequency (GHz)**	S_{11} **(dB)**
11.24	−25.16	11.45	−20.91
12.98	−29.36	12.91	−26.19
13.48	−26.02	13.20	−18.94
Broad-band Bandwidth: 1.50 GHz		**Broad-band Bandwidth: 0.91 GHz**	

connected to the VNA. A horn antenna served as the receiving antenna in the anechoic environment, while the MRPMGS antenna served as the transmitting antenna. The two antennas were positioned at a distance of roughly one meter.

To reduce the influence of near-far field and diffraction effects on the measurements, the MRPMGS antenna being tested is placed in front of the receiving antenna. The computer feeds instructions to the revolving MRPMGS antenna and the horn

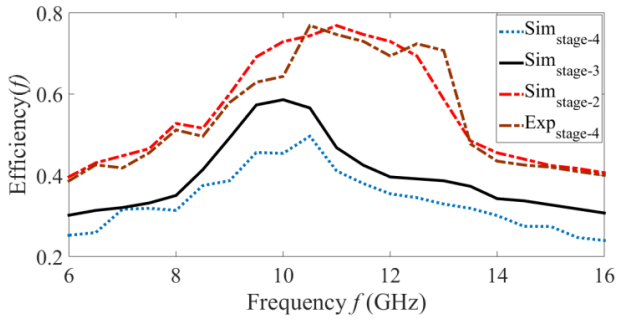

FIGURE 17. Experimentally measured and simulated radiation efficiencies of the MRPMGS antenna.

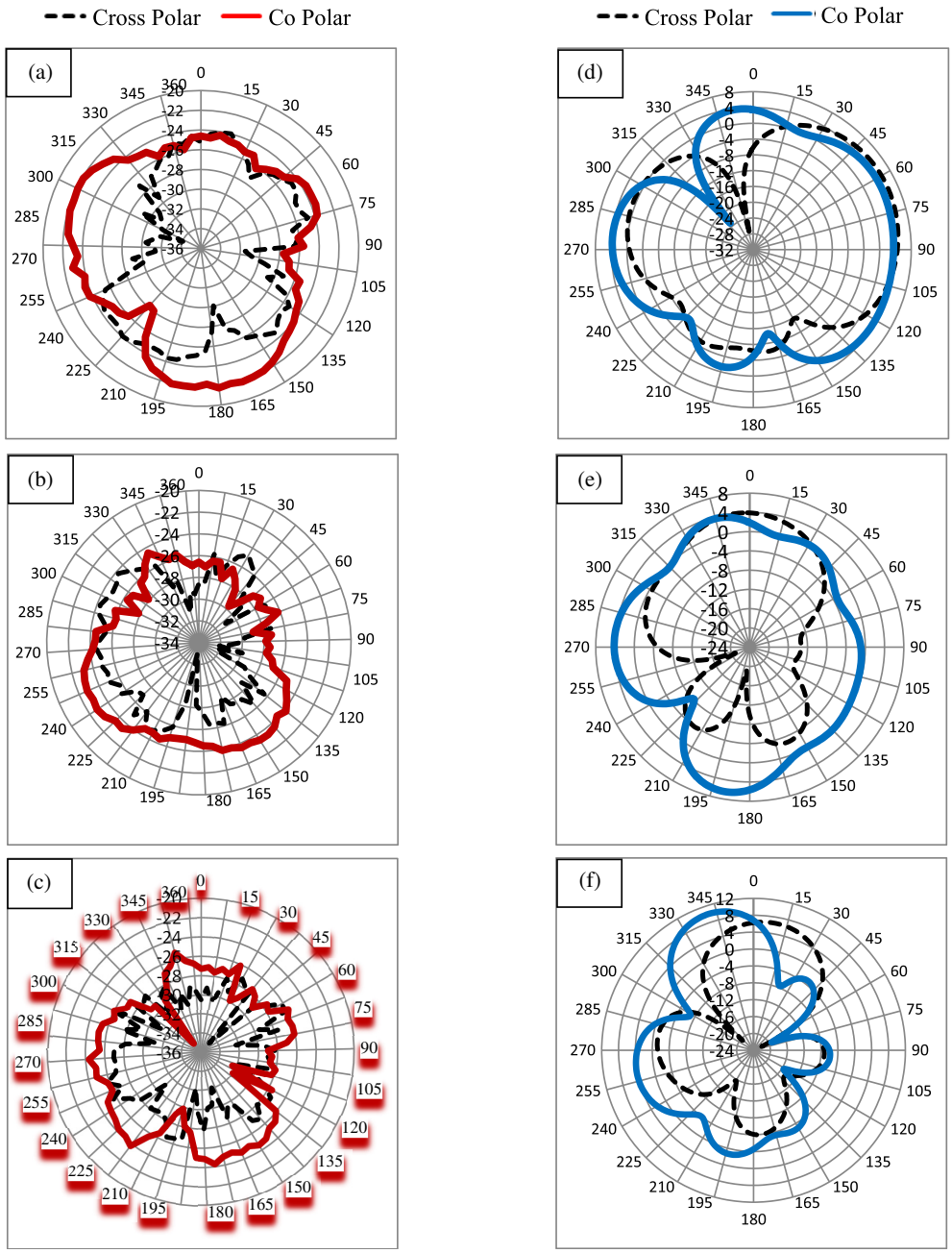

FIGURE 18. Experimentally measured co-polar and cross-polar radiation patterns at (a) 11.54 GHz, (b) 12.91 GHz, (c) 13.20 GHz. Simulated co polar and cross polar radiation patterns at (d) 11.24 GHz, (e) 12.98 GHz, (f) 13.48 GHz.

TABLE 3. Comparison of performance measures of the proposed MRPMGS antenna with reported design(s).

Ref.	Overall patch size mm^3	Unit cell size top layer (mm)	Count	DGS unit cell size bottom layer (mm)	Count	Type/ Arch./ Topology	Freq. bands (GHz)	Broad-band (GHz) (−10 dB)	Gain (max) (dB)	Rad. Eff. (%)	Rad. Pattern
[16]	$50 \times 30 \times 1$ $1.166\lambda_o \times 0.699\lambda_o$ $\times 0.23\lambda_o$	–	–	6×6	16 (CSR)	MTM based DGS	2.4, 5.9, 7.8, 10.12	–	3.8	95	Dir.
[17]	$91.62 \times 53.93 \times 1.6$ $0.255\lambda_o \times 0.155\lambda_o$ $\times 0.012\lambda_o$	33.30×20.22	4 (CRR)	–	–	MTM based radiating patch	2.26	–	5.1	95.66	Dir.
[19]	$50 \times 44 \times 1.6$ $0.816\lambda_o \times 0.718\lambda_o$ $\times 0.026\lambda_o$	3.03×2.09	06 (CSRR)	–	–	MTM based radiating patch	4.9	0.16	–	67	Omni
[21]	$37 \times 44 \times 1.6$ $0.493\lambda_o \times 0.586\lambda_o$ $\times 0.0213\lambda_o$	16×14	01 (CFL)	–	–	MTM based radiating patch	3.2	1.156	2.28	75	Dir.
[22]	$100 \times 100 \times 3$ $1.78\lambda_o \times 1.78\lambda_o$ $\times 0.053\lambda_o$	–	–	3.9×3.9	02 (CSRR)	MTM based DGS	1.93, 3.73, 4.35, 6.35, 7.25	0.6	9.9	–	Omni
[25]	$21 \times 21 \times 2$ $0.544\lambda_o \times 0.544\lambda_o$ $\times 0.052\lambda_o$	–	–	2.1 & 2.35 3.68 & 3.93 1.93 & 2.35 2.85 & 3.20	04 (CRR)	MTM based DGS	7.65, 7.90	0.91	–	–	Omni
[29]	$31 \times 25 \times 1.6$ $0.287\lambda_o \times 0.231\lambda_o$ $\times 0.014\lambda_o$	5×5	4 (MSR)	–	–	MTM based radiating patch	2.78, 5.88	–	–	–	Omni
[30]	$10.3 \times 10.3 \times 0.7$ $1.1\lambda_o \times 1.1\lambda_o$ $\times 0.077\lambda_o$	10.3×10.3	01	–	–	MTM based radiating patch	27.67, 29.07, 33.73	2.23	5.5	97	Omni
[35]	$40 \times 40 \times 1.6$ $0.413\lambda_o \times 0.413\lambda_o$ $\times 0.016\lambda_o$	–	–	6×4	16 (SRR)	MTM based DGS	3.1, 4.4	–	6.34	90	Dir.
Proposed	$12 \times 16 \times 0.8$ $0.529\lambda_o \times 0.705\lambda_o$ $\times 0.035\lambda_o$	4×4 2.8×2.8 0.8	12 (IRR)	3.6×3.6 2.8×2.8	30 CRR	MTM based radiating patch & MTM based DGS	11.45, 12.91, 13.20	0.91	5.5	80	Omni

CSR: continuous spiral resonator CRR: close ring resonator MSRR: multiple split ring resonator CSRR: complementary split ring resonator CRR: concentric ring resonator CFL: continuous fold line IRR: interconnected ring resonator

antenna positioned front to front, polarizing the E-field and H-field in co-planar and cross-planar orientations in order to measure the radiation patterns. In a cross-planar configuration, the MRPMGS and horn antennas are orthogonal to one another with regard to E-field and H-field orientations, whereas in a co-planar position, they are aligned in the same direction. The resonance frequencies of the proposed MRPMGS antenna are measured experimentally and compared to the simulated findings, which meet the −10 dB requirements, as illustrated in Fig. 15. There is a small discrepancy between the simulated and measured results, which could be the result of fabrication flaws. The gain is measured experimentally which is observed to vary from 2.35 to 5.5 shown in Fig. 16, and it is in close resemblance with the simulated values. Fig. 17 depicts the comparison of simulated radiation efficiency for Stage-2, Stage-3, and Stage-4. It clearly shows the improvement with the addition of metamaterial based unit cells in radiating patch and DGS. For Stage-4, the simulated radiation efficiency is compared with the measured values and found to be in close resemblance.

The comparison of experimentally measured and simulated radiation patterns is shown in Figs. 18(a)–18(f) using 2D polar plots of MRPMGS antenna at resonance frequencies of 11.54 GHz (11.24 GHz), 12.91 GHz (12.98 GHz), and 13.20 GHz (13.48 GHz). The orientation of MRPMGS antenna

is in xy-plane. Electric field strength is in the z-direction for antenna to be in co-plane ($\varphi = 0$); the antenna, when orients in the cross-plane ($\varphi = 90$), becomes orthonormal with respect to the co-plane. Both co-polarization and cross-polarization lead to an inverted orientation of the electric field. The MRPMGS antenna's far field radiation patterns are simulated at 11.24 GHz, 12.98 GHz, and 13.48 GHz and shown in Figs. 18(d), 18(e), and 18(f). The 2D radiation patterns so obtained experimentally are depicted in Figs. 18(a), 18(b), and 18(c). For both generated and empirically observed findings, the radiation patterns exhibit omnidirectional features that make it appropriate for wireless and ITS applications.

The concept of unit cells with different optimized structures is also used in transmitarray antennas with multiple layers [33, 34] which act as phase shifting surfaces (PSSs), to achieve wide bandwidth and high gain in antennas. However, the use of multiple layers results in increased insertion losses, thickness, and requires mechanical screws support. In the presented manuscript, the metamaterial unit cells are single layered on the top surface and on the bottom ground surface (DGS). The concept of unit cells on the top and bottom surfaces results in appreciable high gain, wide bandwidth, and high efficiency.

6. CONCLUSION

A three layered novel patch antenna design that is distinguished by its metamaterial unit cell-based ground structure and radiating patch on top is simulated, fabricated, and experimentally tested. The antenna design is simulated in CST Microwave studio splitting the antenna structure into 588,570 hexahedral mesh cells. The design is optimized in four stages. The design in Stage-1 is a conventional rectangular patch with the complete ground plane at the bottom. In Stage-2, the conventional rectangular patch on top is modified with metamaterial unit cells based patch. In Stage-3, the defects are added in ground plane in terms of horizontal and vertical etchedlinear patches. In Stage-4, the DGS is further modified to metamaterial based unit cells. The unique design resonates at 11.54 GHz, 12.91 GHz, and 13.20 GHz. The uniqueness in the antenna design with loaded metamaterial unit cells resulted in broad-band response where the second and third resonance bands merged to have a -10 dB bandwidth of 0.91 GHz. The proposed antenna exhibited VSWR in between 1 and 3. The gain is in between 2.35 and 5.5 for desired frequencies. The radiation efficiency reached 80% in the proposed antenna design. The unique design also resulted in the suppression of back and side lobes to a great extend. The performance of the proposed antenna is compared with reported designs, and the comparison is summarized in Table 3. The comparison table clearly depicts that the reported designs have either top layer loaded with metamaterial unit cells or ground plane loaded with metamaterial unit cells. The proposed antenna design is novel with both top layer (radiating patch) and bottom layer (ground plane) loaded with metamaterial unit cells. With this novel design, the MRPMGS antenna exhibited relatively small size, high gain (5.5 dB), high radiation efficiency (80%), simulated broad-band (1.5 GHz), and measured broad-band (0.91 GHz) with omnidirectional radiation patterns.

REFERENCES

[1] Gupta, S. D. and M. C. Srivastava, "Design of frequency agile multidielectric microstrip antenna for airborne applications," *International Journal of Microwave and Optical Technology (IJMOT)*, Vol. 5, No. 5, 257–266, 2010.

[2] Wu, J., J. Yu, and Q. Tao, "Design of a missile-borne conformal microstrip navigation antenna," *MATEC Web of Conferences*, Vol. 232, 04080, 2018.

[3] Chattha, H. T., M. Hanif, X. Yang, I. E. Rana, and Q. H. Abbasi, "Frequency reconfigurable patch antenna for 4G LTE applications," *Progress In Electromagnetics Research M*, Vol. 69, 1–13, 2018.

[4] Khattak, M. I., A. Sohail, U. Khan, Z. Barki, and G. Witjaksono, "Elliptical slot circular patch antenna array with dual band behaviour for future 5G mobile communication networks," *Progress In Electromagnetics Research C*, Vol. 89, 133–147, 2019.

[5] Alieldin, A., Y. Huang, S. J. Boyes, and M. Stanley, "A reconfigurable broadband dual-mode dual-polarized antenna for sectorial/omnidirectional mobile base stations," *Progress In Electromagnetics Research*, Vol. 163, 1–13, 2018.

[6] Zhang, Q., W. Jiang, P. Liu, K. Wei, W. Hu, and S. Gong, "Metamaterial-based linear phased array antenna with improved wide-angle scanning bandwidth by parasitic metal strips," *IET Microwaves, Antennas & Propagation*, Vol. 15, 1699–1709, 2021.

[7] Naik, K. K. and P. A. V. Sri, "Design of hexadecagon circular patch antenna with DGS at Ku band for satellite communications," *Progress In Electromagnetics Research M*, Vol. 63, 163–173, 2018.

[8] Saroj, A. K., M. G. Siddiqui, M. Kumar, and J. Ansari, "Design of multiband quad-rectangular shaped microstrip antenna for wireless applications," *Progress In Electromagnetics Research M*, Vol. 59, 213–221, 2017.

[9] Jabar, A. A. S. A. and D. K. Naji, "Design of miniaturized quad-band dual-arm spiral patch antenna for RFID, WLAN and WiMAX applications," *Progress In Electromagnetics Research C*, Vol. 91, 97–113, 2019.

[10] Khajepour, S., M. S. Ghaffarian, and G. Moradi, "Design of novel multiband folded printed quadrifilar helical antenna for GPS/WLAN applications," *Electronics Letters*, Vol. 53, No. 2, 58–60, 2017.

[11] Sun, X., G. Zeng, H.-C. Yang, Y. Li, X.-J. Liao, and L. Wang, "Design of an edge-fed quad-band slot antenna for GPS/WiMAX/WLAN applications," *Progress In Electromagnetics Research Letters*, Vol. 28, 111–120, 2012.

[12] Yu, J., Y. Sun, H. Zhu, F. Li, and Y. Fang, "Stacked-patch dual-band & dual-polarized antenna with broadband baluns for WiMAX & WLAN applications," *Progress In Electromagnetics Research M*, Vol. 68, 41–52, 2018.

[13] Liu, C.-S., C.-N. Chiu, and S.-M. Deng, "A compact disc-slit monopole antenna for mobile devices," *IEEE Antennas and Wireless Propagation Letters*, Vol. 7, 251–254, 2008.

[14] Kishore, N., A. Prakash, and V. S. Tripathi, "A reconfigurable ultra wide band antenna with defected ground structure for ITS application," *AEU — International Journal of Electronics and Communications*, Vol. 72, 210–215, 2017.

[15] Kishore, N., G. Upadhyay, V. S. Tripathi, and A. Prakash, "Dual band rectangular patch antenna array with defected ground structure for ITS application," *AEU — International Journal of Electronics and Communications*, Vol. 96, 228–237, 2018.

[16] Alqadami, A. S. M., M. F. Jamlos, I. Islam, P. J. Soh, R. Mamat, K. A. Khairi, and A. Narbudowicz, "Multi-band antenna array based on double negative metamaterial for multi automotive applications," *Progress In Electromagnetics Research*, Vol. 159, 27–37, 2017.

[17] Mishra, N. and R. K. Chaudhary, "A compact CPW fed CRR loaded four element metamaterial array antenna for wireless application," *Progress In Electromagnetics Research*, Vol. 159, 15–26, 2017.

[18] Weng, W.-C. and C.-L. Hung, "An H-fractal antenna for multiband applications," *IEEE Antennas and Wireless Propagation Letters*, Vol. 13, 1705–1708, 2014.

[19] Song, Z., S. Zhao, S. Li, J. Chen, and Y. Xue, "High-isolation compact MIMO antenna with distributed metamaterial loading," *Progress In Electromagnetics Research M*, Vol. 128, 51–59, 2024.

[20] Naik, K. K., G. Dattatreya, R. P. S. Chaitanya, R. Palla, and S. S. Rani, "Enhancement of gain with corrugated Y-shaped patch antenna for triple-band applications," *International Journal of RF and Microwave Computer-Aided Engineering*, Vol. 29, No. 3, e21624, 2019.

[21] Mood, Y. and R. Pandeeswari, "Complementary folded line metamaterial loaded MIMO antenna for S-band applications," *Progress In Electromagnetics Research C*, Vol. 150, 145–155, 2024.

[22] Upadhyay, G., N. Kishore, S. Raj, S. Tripathi, and V. S. Tripathi, "Dual-feed CSRR-loaded switchable multiband microstrip patch antenna for ITS applications," *IET Microwaves, Antennas & Propagation*, Vol. 12, No. 14, 2135–2140, 2018.

[23] Kakhki, M. B. and P. Rezaei, "Reconfigurable microstrip slot antenna with DGS for UWB applications," *International Journal of Microwave & Wireless Technologies*, Vol. 9, No. 7, 1517–1522, 2017.

[24] Ziolkowski, R. W. and A. Erentok, "Metamaterial-based efficient electrically small antennas," *IEEE Transactions on Antennas and Propagation*, Vol. 54, No. 7, 2113–2130, 2006.

[25] Upadhyay, K. K., A. Agrawal, and M. Misra, "Wide-band log-periodic microstrip antenna with defected ground structure for C-band applications," *Progress In Electromagnetics Research C*, Vol. 112, 127–137, 2021.

[26] Veselago, V. G., "The electrodynamics of substances with simultaneously negative values of ε and μ," *Soviet Physics Uspekhi*, Vol. 10, No. 4, 509, 1968.

[27] Pendry, J. B., A. J. Holden, D. J. Robbins, and W. J. Stewart, "Magnetism from conductors and enhanced nonlinear phenomena," *IEEE Transactions on Microwave Theory and Techniques*, Vol. 47, No. 11, 2075–2084, 1999.

[28] Smith, D. R., W. J. Padilla, D. C. Vier, S. C. Nemat-Nasser, and S. Schultz, "Composite medium with simultaneously negative permeability and permittivity," *Physical Review Letters*, Vol. 84, No. 18, 4184, 2000.

[29] Selvi, N. T., R. Pandeeswari, and P. N. T. Selvan, "An inset-fed rectangular microstrip patch antenna with multiple split ring resonator loading for WLAN and RF-ID applications," *Progress In Electromagnetics Research C*, Vol. 81, 41–52, 2018.

[30] Hassan, K. M. Z., N. Wongkasem, and H. Foltz, "A Ka-band omnidirectional metamaterial-inspired antenna for sensing applications," *Sensors*, Vol. 25, No. 11, 3545, 2025.

[31] Jackson, D. R. and N. G. Alexopoulos, "Simple approximate formulas for input resistance, bandwidth, and efficiency of a resonant rectangular patch," *IEEE Transactions on Antennas and Propagation*, Vol. 39, No. 3, 407–410, 1991.

[32] Agrawal, A., M. Misra, and A. Singh, "Oblique incidence and polarization insensitive multiband metamaterial absorber with quad paired concentric continuous ring resonators," *Progress In Electromagnetics Research M*, Vol. 60, 33–46, 2017.

[33] Tuloti, S. H. R., P. Rezaei, and F. T. Hamedani, "Unit cell with flexible transmission phase slope for ultra-wideband transmitarray antennas," *IET Microwaves, Antennas & Propagation*, Vol. 13, No. 10, 1522–1528, 2019.

[34] Tuloti, S. H. R., P. Rezaei, and F. T. Hamedani, "High-efficient wideband transmitarray antenna," *IEEE Antennas and Wireless Propagation Letters*, Vol. 17, No. 5, 817–820, 2018.

[35] Chandrasekhar, M. and K. K. Naik, "Design a dual-band with CSRR cascaded patch antenna array for wireless communications," *Progress In Electromagnetics Research C*, Vol. 149, 155–163, 2024.